

# Dynamic Active Sites In Situ Formed in Metal Nanoparticle Reshaping under Reaction Conditions

Xiao-Yan Li, Pengfei Ou, Xinyi Duan, Lei Ying, Jun Meng, Beien Zhu,\* and Yi Gao\*



Cite This: *JACS Au* 2024, 4, 1892–1900



Read Online

ACCESS |

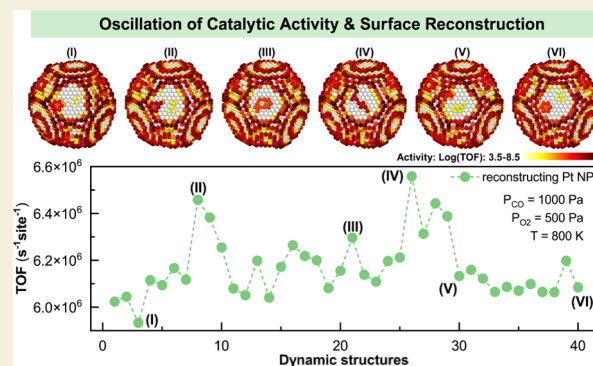
Metrics & More

Article Recommendations

Supporting Information

**ABSTRACT:** Understanding the nonequilibrium transformation of nanocatalysts under reaction conditions is important because metastable atomic structures may be created during the process, which offers unique activities in reactions. Although reshaping of metal nanoparticles (NPs) under reaction conditions has been widely recognized, the dynamic reshaping process has been less studied at the atomic scale. Here, we develop an atomistic kinetic Monte Carlo model to simulate the complete reshaping process of Pt nanoparticles in a CO environment and reveal the in situ formation of atomic clusters on the NP surface, a new type of active site beyond conventional understanding, boosting the reactivities in the CO oxidation reaction. Interestingly, highly active peninsula and inactive island clusters both form on the (111) facets and interchange in varying states of dynamic equilibrium, which influences the catalytic activities significantly. This study provides new fundamental knowledge of nanocatalysis and new guidance for the rational design of nanocatalysts.

**KEYWORDS:** active site, surface roughening, CO oxidation, environmental kinetic Monte Carlo, structure sensitivity



This study provides new fundamental knowledge of nanocatalysis

## 1. INTRODUCTION

The structure of a metal catalyst plays a critical role in determining its activity.<sup>1–3</sup> In recent years, in situ experiments have demonstrated that the structures of catalysts undergo dramatic reconstructions in changing gaseous environments.<sup>4–6</sup> A typical example is the reshaping of metal nanoparticles (NPs) under reaction conditions, which has attracted much attention because the number of active sites would be changed, and new active sites could also be created during the structural transformation.<sup>7</sup> Since Hansen et al. reported the water vapor-induced reversible reshaping of supported Cu NPs, this type of interesting phenomenon has been studied by in situ microscopies and theoretical modeling for over 20 years.<sup>8</sup> A plethora of dynamic shape changes have been observed in NPs (Pt,<sup>9</sup> Pd,<sup>10–13</sup> PdCu,<sup>14</sup> Au<sup>15</sup>) under different reactive environments. Despite these achievements,<sup>16,17</sup> studies of the dynamic evolution of the reshaping process at the atomic scale are limited. The lack of knowledge of atomistic transformations hinders a comprehensive understanding of the true atomic surface structures of NP in reactions.

Although many theoretical methods to model the structure reconstruction of catalysts have been developed in recent years with ever-growing computational power, a new model is essential to accurately represent the structural changes of catalysts at the atomic scale.<sup>18,19</sup> Recent theoretical modeling techniques have been established to predict the equilibrium

structures of metal NPs and nanoclusters under reaction conditions from a thermodynamic perspective.<sup>20–22</sup> However, these studies focused on the equilibrium structures that cannot fully represent the nonequilibrium changes of catalysts in reactive environments. The combination of quantum chemical calculations, machine learning algorithms, and molecular dynamics methods allows for the atomic simulation of catalytic interfaces consisting of dozens to hundreds of atoms up to nanoseconds.<sup>23–25</sup> But the spatial and temporal scales are still too small to study the reshaping process. Conventional kinetic Monte Carlo (KMC) models have been developed to study the growth and dissolution of metal NPs under a vacuum or in a liquid environment.<sup>26–28</sup> However, how to take the complexity of the reactive gas effect into consideration is a question.

In this work, we present an atomistic KMC model that can well describe the complicated migration behaviors of different surface atoms of NP under the reaction conditions. Using this model, we realized the simulation of the reshaping process of a Pt NP under CO gas conditions and unraveled the in situ

**Received:** January 30, 2024

**Revised:** April 11, 2024

**Accepted:** April 12, 2024

**Published:** May 9, 2024



formation of atomic clusters, mainly on the (111) facets, during the reshaping process. We currently choose CO as a typical reaction condition because previous experiments have shown the dominant effects of CO on the structures of catalysts in mixed gaseous environments, including CO and O<sub>2</sub> gas mixtures.<sup>7</sup> We further show that the mechanism of the in situ cluster formation is closely related to the reshaping process, which is different from the mechanisms of in situ adatom formation on crystal surfaces.<sup>29,30</sup> Through reaction activity simulation and mechanistic analysis, we found there are two types of in situ-formed clusters on NP: the isolated island is inactive and the peninsula is highly active in the CO oxidation reaction. Conventional studies have widely used well-defined polyhedrons as models of NPs, in which the active sites are commonly attributed to the low-coordinated corners and edges.<sup>31</sup> Here, we demonstrate the in situ-formed clusters as a new type of active site on the NP surface boosting the catalytic activity that has long been overlooked. This new finding provides new perspectives to understand various phenomena of nanocatalysis, including reaction oscillation and high activity of terrace facets. This also provides new guidance for the rational design of metal catalysts.

## 2. METHODS

### 2.1. Kinetic Monte Carlo Simulation Methods

Gillespie's direct method (DM) was adopted as the KMC algorithm within a lattice model of the face-centered cube.<sup>32</sup> In the whole heterogeneous catalytic system, the state could be changed by the adsorption, desorption, and diffusion of gas molecules and adsorbed species on the catalyst surface as well as the migration of catalyst atoms with the potentially adsorbed species.

The time ( $\Delta t$ ) of the current system taken to reach from one state to another is evaluated as follows<sup>33</sup>

$$\Delta t = \frac{\ln(u_1)}{k_{\text{tot}}} \quad (1)$$

$$k_{\text{tot}} = \sum_{\text{site}=1} \sum_{j=1} k_a \quad (2)$$

where  $u_1$  is a random number in the interval  $[(0, 1)]$ ,  $k_{\text{tot}}$  is the sum of the rate constants of possible events in the simulation, and  $k_a$  is an executed process (an event occurring at a lattice site).

In each KMC step, after the rate constants of all possible events are calculated, one event is stochastically selected to occur according to the proportion of the event's rate constant to the total rate constant, described as follows<sup>34</sup>

$$k_1 + k_2 + \dots + k_a \leq u_2 k_{\text{tot}} \leq k_1 + k_2 + \dots + k_a + k_{a+1} \quad (3)$$

where  $k_a$  is the rate constant of every event and  $u_2$  is a random number of  $[(0, 1)]$ . Then, the list of possible rate constants ( $k$ ) is updated after each step. The calculation of rate constants is described in the [Supporting Information](#).

To simulate the surface reconstruction under reaction conditions precisely and efficiently, we describe the energy of the catalyst system ( $E$ ) as a function of the generalized coordination number ( $\text{GCN}_i$ ) and coordination number ( $\text{CN}_i$ ) of each site  $i$ , which includes the metal–metal interactions ( $E_{\text{MM}}$ ) and the metal–gas interaction ( $E_{\text{ads}}$ )<sup>35,36</sup>

$$E = \sum_i E_{\text{MM}}^i(\text{CN}_i, \text{GCN}_i) + \sum_i E_{\text{ads}}^i(\text{GCN}_i) \quad (4)$$

where the first term of  $E_{\text{MM}}^i$  is a Hubbard-model-like definition

$$E_{\text{MM}}^i = \frac{1}{2} \varepsilon_{\text{M}} \text{CN}_i + U_0 \delta_i \quad (5)$$

where  $\varepsilon_{\text{M}}$  is the bond energy obtained by fitting the surface energy according to our previous works.<sup>35,37</sup>  $U_0$  is the constant cohesive energy derived from the periodic bulk metal system, and  $\delta_i$  is the scaling factor to correct the cohesive energy of the catalyst with different sizes (from a single atom to a periodic bulk system). The second term of  $E_{\text{ads}}^i$  was described using the scaling relationship with GCN, as proposed by Calle-Vallejo et al., which has been proven to be an effective way for describing the Pt–gas interactions in previous literature.<sup>38,39</sup>

For the atomic migration in the reconstruction process, we could effectively evaluate the energy barrier ( $E_a^{\text{mig}}$ ) of the atomic migration on the catalyst surface with the adsorption of gas molecules as follows<sup>28</sup>

$$E_a^{\text{mig}} = (E_f - E_b) - \frac{E_f}{E_f + E_b} \frac{E_f^2}{E_f^2 + E_b^2} E_f \quad (6)$$

where  $E_f$  and  $E_b$  are the formation energy and broken energy after and before atomic migration. Considering the adsorption and repulsion of intermediates on the catalyst surface, the rationality of choosing eq 6 is verified by comparison with density functional theory (DFT) calculations (Table S1). Within our theoretical framework, surface atom migration naturally follows the following rules: (1) without the adsorption of gas, the migration of a highly coordinated atom to a low-coordinated site is difficult; (2) gas adsorption reduces the value of  $E_a^{\text{mig}}$  for one surface atom moving from a high-coordinated site to a low-coordinated site because of enhanced adsorption and reduced repulsion on the latter; and (3) gas adsorption also reduces the  $E_a^{\text{mig}}$  of a surface adatom on terrace sites. All of these rules are composed of the physical origin of the structural reconstruction under the reaction conditions. More derivations and details for KMC simulations are provided in the [Supporting Information](#).

### 2.2. Density Functional Theory Calculations

All spin-unrestricted density functional theory (DFT) calculations were performed utilizing the Vienna Ab-Initio Simulation Package (VASP).<sup>40</sup> The projector-augmented wave method (PAW) was used with valence electron numbers of Pt(10), O(6), and C(4).<sup>41</sup> The cutoff energy was 400 eV for the plane-wave expansion. We adopted the revised Perdew–Burke–Erzernhof functional in the generalized-gradient approximation (GGA-RPBE).<sup>42,43</sup> The functional developed by Hammer et al. is to improve the accuracy of adsorption energy of small molecules (NO, CO, etc.) on the noble-metal surfaces (Pt, Rh, etc.),<sup>44,45</sup> which has been extensively validated and applied.<sup>21,22</sup> For the optimization of geometry structure, the convergences of the electronic self-consistent energy and forces must be less than  $10^{-5}$  eV and 0.05 eV/Å for the structural optimization, respectively.

Here, all periodic two-dimensional (2D) surfaces were built from an optimized faced-centered cubic (FCC) cell with a lattice parameter of 4.0 Å. The vacuum space is 15 Å to separate the slabs along the  $z$ -axis. The bottom two atomic layers are fixed to mimic the bulk structure. The top four atomic layers are allowed to relax. For the search of the transition state in CO oxidation, CO diffusion, O diffusion, and Pt atomic migration on the Pt surface, the climbing image nudged elastic band (CI-NEB) method was performed using the VTST module of VASP.<sup>46</sup> The transition states are optimized until all force and electronic self-consistent energy criteria are less than 0.05 eV/Å and  $10^{-5}$  eV, respectively.

Periodic ( $4 \times 4$ ) slabs were used to calculate the adsorption energy and reaction barrier of In CO oxidation. The  $k$ -point grid was ( $3 \times 3 \times 1$ ).<sup>47</sup> To calculate the average repulsive energies of adsorbed species, the periodic ( $1 \times 1$ ) slabs with a full surface coverage were applied for the average repulsive energies of CO–CO and O–O, where the  $k$ -point grid was ( $8 \times 8 \times 1$ ).<sup>47</sup> The average repulsive energy of CO–O was calculated on the periodic ( $2 \times 2$ ) slab with a full surface coverage, where the  $k$ -point was ( $4 \times 4 \times 1$ ).<sup>47</sup>

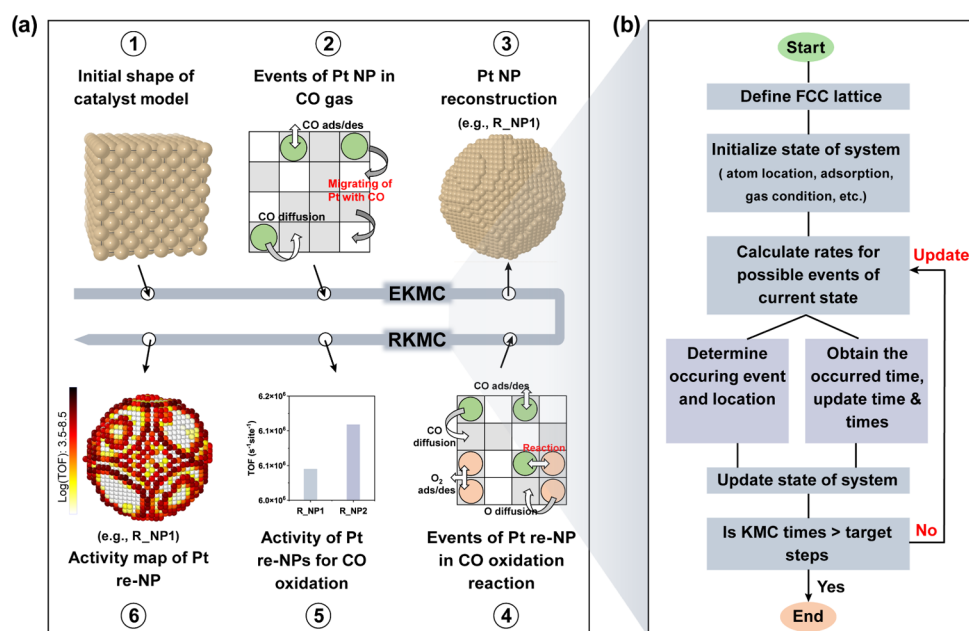


**Figure 1.** Chart flow for studying the effect of gaseous environment on catalyst's structure and performance. (a) Starting from an initial model with arbitrary morphology, the reconstructed NP structure (e.g., R\_NP1) is sampled using the EKMC procedure, considering the possible events of Pt NP in CO gas. Using the sampled structure as a model, the performed RKMC simulation enables us to estimate the activity (i.e., 3D activity map and TOF) of Pt NP toward the CO oxidation reaction. (b) KMC algorithm with a lattice model of a face-centered cube.

### 3. RESULTS AND DISCUSSION

#### 3.1. Theoretical Protocol of Dual KMC Approaches

We depict the proposed theoretical protocol of our study in Figure 1a, using a combination of dual KMC approaches and DFT calculations. In the environmental KMC (EKMC, steps 1–3) simulation, we start with a model using a well-defined morphology as the initial structure, and then consider the elementary steps of gas adsorption, desorption, diffusion on the NP surface, and particularly the migration of surface atoms of the NP at a given temperature and pressure. The migration of Pt surface atoms reshapes the morphology of the NP and further roughens the surface simultaneously. The reconstructed NP (R\_NP) obtained from EKMC is adopted as the model for the reactive KMC (RKMC, steps 4–6) simulation, where the catalytic activity is evaluated by considering the adsorption, desorption, diffusion, and reaction of the adsorbed species. The algorithm of the dual KMC approach is presented in Figure 1b. This protocol facilitates the study of the influence of the surrounding environment on the surface structure and catalytic performance of nanoscale catalysts on the atomic scale.

#### 3.2. Modeling the Self-Generation of Clusters on the Facets of Pt NP in the Reaction Environment

Using the EKMC approach, we examined the morphological transformation of a Pt nanocube of  $\sim 4$  nm (5324 atoms) under a CO pressure of 1000 Pa. The temperature was set to 800 K to accelerate the structural changes. We performed simulations over  $2 \times 10^9$  KMC steps ( $>0.5$  ms) for the system to reach a quasi-equilibrium state. Figure 2a illustrates some snapshots of the reconstructed NP structures versus the simulation time to directly visualize the NP reconstruction process. It was observed that the atoms from the edges and corners migrated over the (100) facets to expose the (111) and (110) facets, leading to surface roughening and a shape change. During structural transformation, the surface-to-

volume ratio of the Pt NP quickly decreased to a dynamic equilibrium state at about 0.20, with an increase in CO coverage from 0.22 to 0.31. The reshaped NP has a rounded shape with exposure of the (110) facets by CO adsorption after approximately 0.408 ms. This morphology change agrees with the experimental observations of Vendelbo et al., in which the high-index facet fractions increased with increasing CO partial pressure during the reaction oscillation.<sup>7</sup> The kinetic simulation results also agree with the thermodynamic predictions in our previous work.<sup>48</sup> Between 0.408 and 0.518 ms, the morphology of the NP did not change significantly, but the surface atom diffusions could still be observed. Particularly, atomic clusters are continuously observed on the NP, as shown in Figure 2b,c. As a comparison, we also performed a similar simulation without CO gas molecules (Figure S11). The morphology of the NP changes but to a truncated octahedron, which is the well-known equilibrium shape of Pt NP under vacuum. Without CO adsorption, fewer adatoms are observed on the NP, and no atomic clusters are formed.

We further evaluated the coverage of CO on the surface sites of different CNs, as shown in Figure S9. The CO coverage on the low CN sites is higher than that on the high-CN sites, which is attributed to the decrease of the CO adsorption energy with an increase of CN. Most of the surface sites with  $CN \leq 6$  are occupied by CO molecules, while few CO molecules adsorb on the (111) facets with  $CN = 9$ . We confirm that the high CO coverage is the main driving force for the structural transformation, as reported in the previous studies.<sup>49,50</sup>

With the examination of the structure of the reshaped Pt NP, there are distinct characteristics on the different facets. NPs are colored by the corresponding CNs to monitor the structural changes and diffusion of surface atoms. We captured three snapshots of the reconstructed Pt NP, as depicted in the left column of Figure 2b. More detailed snapshots focused on the (111) facet are presented in the right column of Figure 2b,

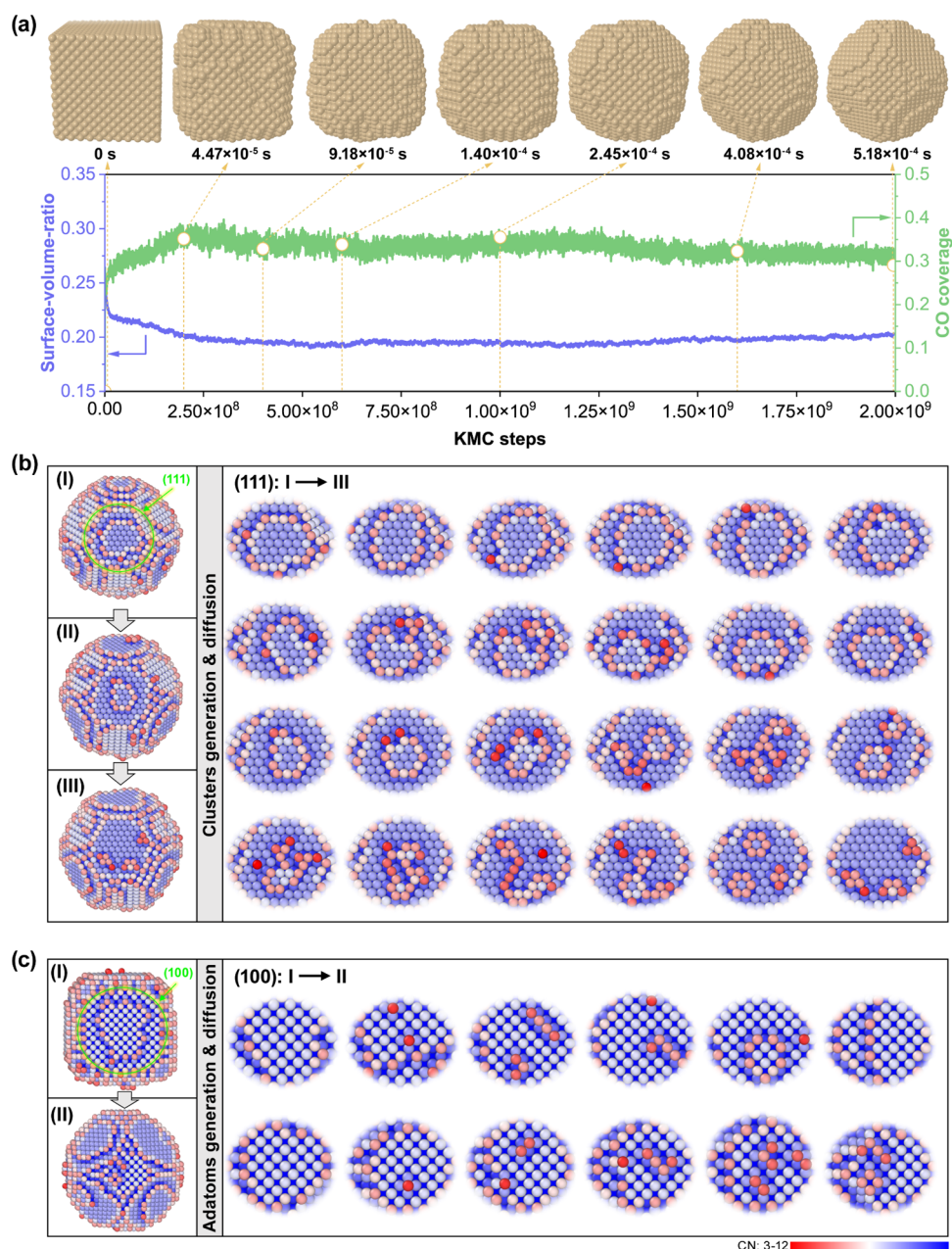


**Figure 2.** Generation of small clusters and adatoms on the reconstructed NP surface. (a) Variations in the surface-to-volume ratio and CO coverage as a function of KMC steps at 800 K. (b, c) KMC snapshots of the reconstructed NP and more detailed snapshots of the (111) and (100) facets.

illustrating the continued migration of edge atoms of the (111) facet to other facets of the NP. Through atom migration, a new and larger (111) facet is exposed, and the shape of the NP evolves to an equilibrium shape. Before the new (111) facet is completely formed, some of the atoms from the old (111) facet stay on the substrate in the form of atomic clusters. These atomic clusters have very low CNs, and form very strong bonds with CO gas molecules that stabilize the clusters on the NP surface after morphology change. Without CO adsorption, these clusters are unstable because their CNs are too low (Figure S11). In the work of Xu et al.,<sup>30</sup> the formation of small clusters on transition metal surfaces in a reactive environment is explained by the ejection of adatoms from steps or kinks to the terraces. Here, we show a completely different mechanism for the in situ formation of atomic clusters on NP facets by

removing atoms from the terrace under the reaction conditions.

Adatoms and their aggregations on the (110) and (100) facets are also observed during the simulation. We captured two NP snapshots to observe changes in (100) facets, as shown in Figure 2c. More detailed snapshots of the (100) facets reveal that the edge atoms of the NP migrated as adatoms to the (100) facets, subsequently gathering into small clusters. The accumulation of atoms forms a new (100) facet with a smaller area. This process continues and cycles, generating new dynamic adatoms on the (100) facets. When the NP evolves to a quasi-equilibrium state, some adatoms and clusters are formed as well on the (100) facets through the mechanism of ejecting adatoms with CO adsorption. As shown in Figure S10, the atoms in (110) facets involved in the edges of the reconstructed NPs dynamically diffuse and tune the size of

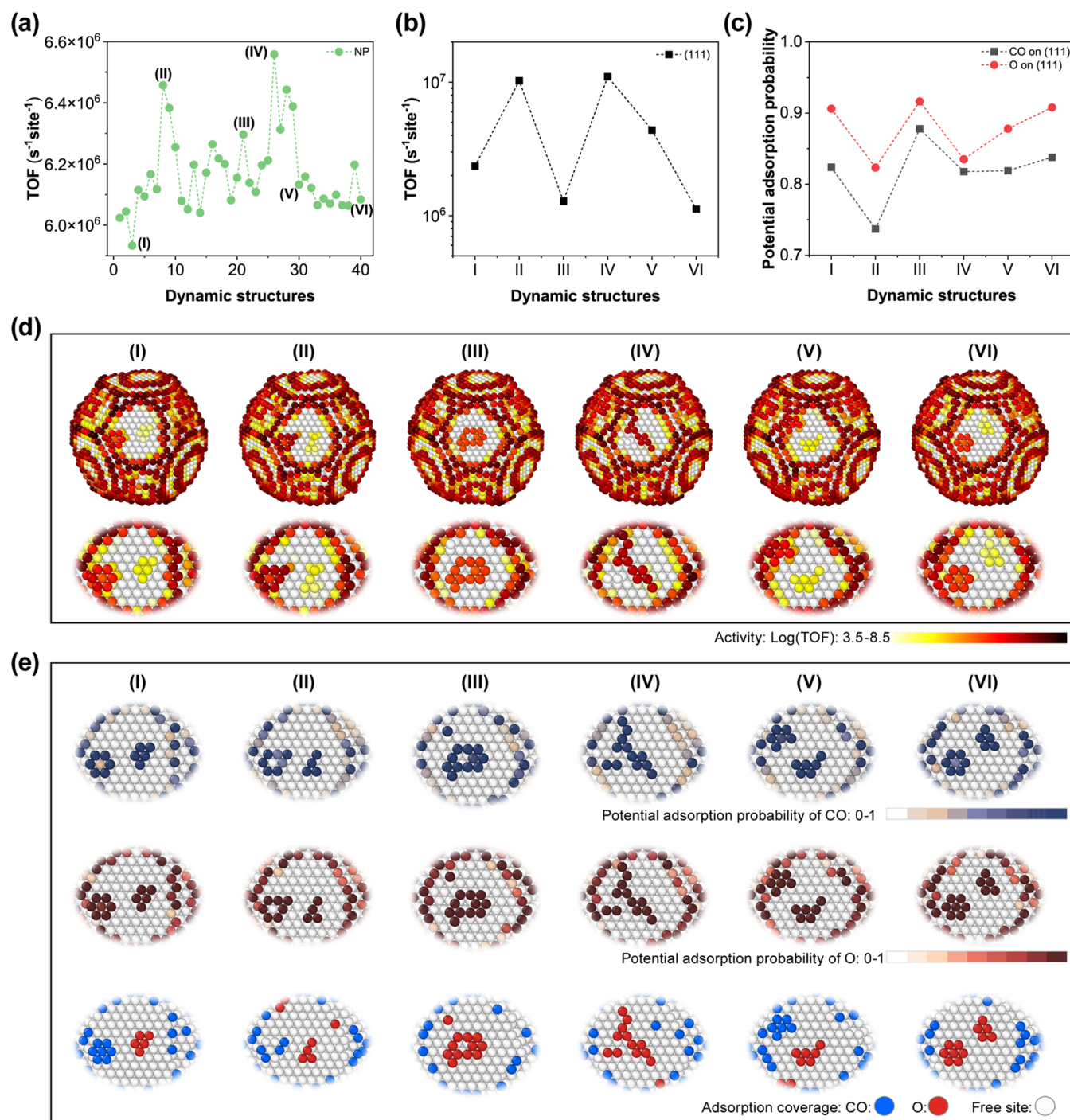


**Figure 3.** Catalytic activity of self-generated clusters. (a) TOF change of 40 dynamically reconstructed NPs, of which 6 NP models are labeled with Roman numerals I to VI. (b) TOFs of (111) facets of NPs at 800 K. (c) TOFs of the (111) facets of NPs. (d) 3D activity maps of NPs and the (111) facets. (e) Maps of potential CO adsorption probability, O adsorption probability, and adsorption coverage on the (111) facets.

(110) facets, in which adatoms (1 and 3 atoms) always dynamically exist on the small (110) facets. The mechanism is similar to that of the (100) facet.

### 3.3. Reactivity Oscillatory Induced by Dynamic Changes in the Size and Location of Clusters

To quantify the activity changes of the dynamically generated atomic clusters over the NP surfaces, we extracted 40 consecutive and 40 reconstructed Pt NP models every 500,000 KMC steps in the last 0.1 billion steps of the EKMC trajectory. We then performed RKMC simulations for

each roughened Pt NP catalyst at 800 K under a CO pressure of 1000 Pa and an  $\text{O}_2$  pressure of 500 Pa. The simulations were all carried out three times with 1.0 billion KMC steps, via turnover frequency (TOF,  $\text{s}^{-1}\text{site}^{-1}$ ), with data from the last 0.5 billion KMC steps collected to analyze the catalytic activity of the overall Pt catalyst (particle TOF) and the respective surface site (site TOF). The catalytic activity changes among different NPs are plotted in Figure 3a, where each value represents the particle TOF relative to the average of all of the TOFs of 40 NPs. These reconstructed NPs show a clear fluctuation in activity at 800 K, with a range as large as  $6.25 \times$

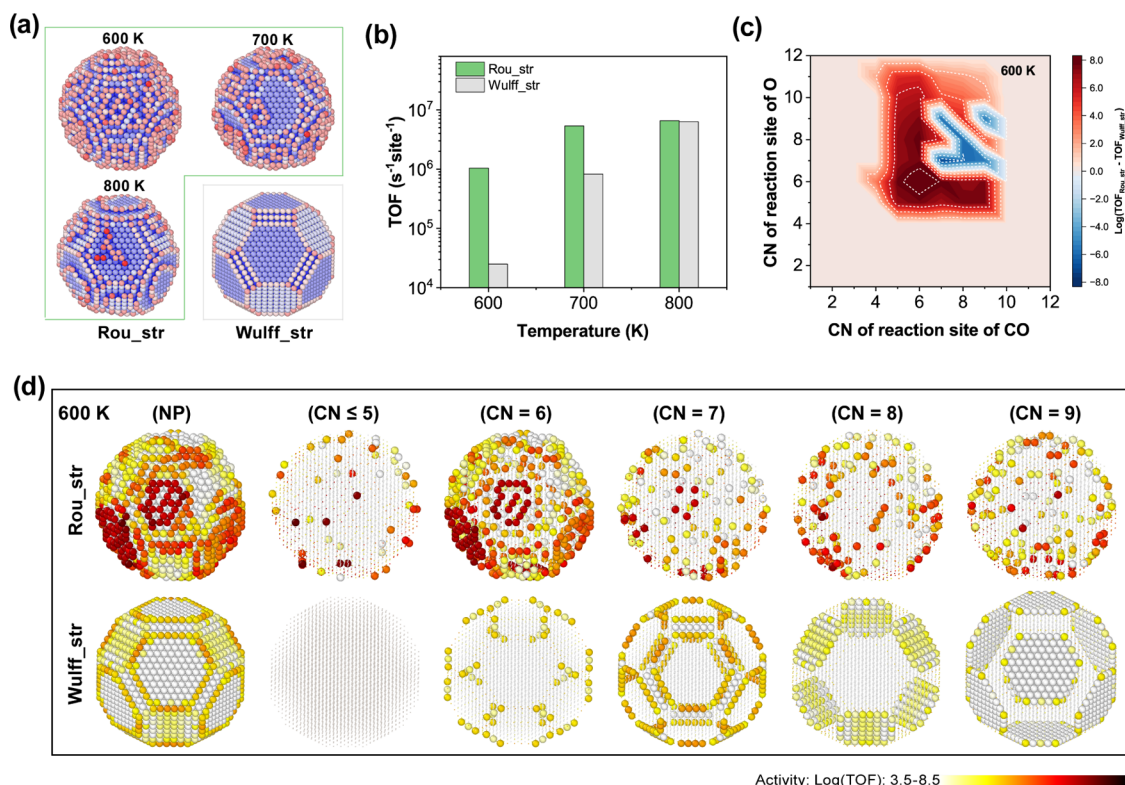


**Figure 4.** Comparison of TOFs of the reconstructed NPs (Rou\_str) and fixed ideal NP (Wulff\_str) at different temperatures. (a) Atomic structures of NPs are colored by the coordination numbers. (b) Particle TOFs of NPs at different temperatures. (c) Difference in 2D activity-CN maps of Rou\_str and Wulff\_str at 600 K. (d) 3D activity-site maps of NPs considering different CNs at 600 K.

$10^5 \text{ s}^{-1} \text{ site}^{-1}$  (from  $5.93 \times 10^6$  to  $6.56 \times 10^6 \text{ s}^{-1} \text{ site}^{-1}$ ), accounting for their dynamic structures.

We chose 6 reconstructed NP models as representatives to show the dynamic changes in the size and location of the clusters on the reconstructed NPs (Figure S12). We focused on the (111) facet because most of the atomic clusters stay on this facet. We observed that the TOFs of small clusters on the (111) facets also present similar trends to the changes of particle TOFs, as shown in Figure 3b. The whole NPs and (111) facets are mapped with different colors based on their site TOF ( $\log(N_{\text{rea}}/s)$ ) to visualize the active site, as shown in Figure 3d. The particle TOFs of the NPs are mainly contributed by the edge atoms and surface clusters with lower CNs. However, we found that not all low CN atoms exhibit high activity. Isolated atoms and atomic clusters (islands) on the (111) facets are almost inactive, whereas clusters connecting with the edges and corners of the NP (peninsulas) exhibit ultrahigh activity.

We presented the statistics of the potential adsorption possibilities of CO or O of atomic clusters on the (111) facets under pure CO and O<sub>2</sub> gas conditions in Figure 3c. These clusters show very high adsorption capacities. We therefore plotted the color maps of the adsorption probability and coverage in Figures 3e and S13. Almost all clusters and atoms show up to 90% adsorption probabilities, indicating the strong adsorption of CO and O on these surface sites. This was proved by the statistics of adsorbed CO and O coverages on the surface sites with different CNs (Figure S14). On the other hand, the substrates of the (111) facets with highly coordinated atoms ( $\text{CN} \geq 9$ ) have difficulty in adsorbing CO or O. Comparing the trend of Figure 3c with that of Figure 3b, we found that the higher CO and O coverages correspond to

lower activities, which indicates that the mechanism of different cluster activities corresponds to the phenomenon of catalytic poisoning. To achieve high activity, CO and O must meet each other frequently. If the catalyst is occupied by only one type of reactant, it will be deactivated, referred to as poisoned. The atomic clusters, no matter whether they are islands or peninsulas, have very limited sites for the adsorption of reactants. There is a high chance that the cluster is covered by the same type of reactant, for example, CO, during the reaction. The cluster itself is poisoned because the strong bonds between the cluster and CO prevent molecule desorption, and no empty sites can be generated for the adsorption of O. The reaction was then stopped. For the island, the nearby substrate site has no adsorbed intermediates to react, resulting in complete catalytic poisoning. For the peninsula, the nearby sites of edges and corners also have a higher adsorption probability of CO or O, resulting in both peninsula atoms and corners showing high activity.

**3.3.1. Contributions of the Self-Generated Clusters to the Nanoparticle Activity.** To fully explore the influence of the self-generated clusters on the catalytic activity, we performed RKMC simulations on the roughened surfaces of the reconstructed NPs (Rou\_str) and the smooth surface of an ideal Wulff NP (Wulff\_str) under a CO pressure of 1000 Pa and an O<sub>2</sub> pressure of 500 Pa at 600, 700, and 800 K. We constructed the Wulff\_str NP with the same diameter of 5.4 nm and a shape similar to that of Rou\_str (Figure S15). The surface-to-volume ratio of Rou\_str (0.20) is also close to that of Wulff\_str (0.21). To determine the structures of Rou\_str NPs at 600 and 700 K, we first carried out EKMC simulations with 200 million KMC steps on the reconstructed surfaces of Pt NPs under a CO pressure of 1000 Pa at 600 and 700 K,

starting with the structure of the reconstructed Pt NP obtained from 800 K simulations to save time. We found that lower temperatures led to the generation of more small clusters and adatoms on the NP surfaces, as shown in Figure 4a. Then, we performed RKM simulation with 1.0 billion KMC steps for these three Rou\_str NPs and Wulff\_str NP under a CO pressure of 1000 Pa and an O<sub>2</sub> pressure of 500 Pa at 600, 700, and 800 K, respectively. Figure 4b depicts the statistics and comparison of the particle TOFs for Rou\_str NPs and Wulff\_str NP at different temperatures. At 800 K, the TOF of Rou\_str is  $6.56 \times 10^6 \text{ s}^{-1} \text{ site}^{-1}$ , which is much higher than that of Wulff\_str ( $6.32 \times 10^6 \text{ s}^{-1} \text{ site}^{-1}$ ). As the temperature decreases, the catalytic activities of both NPs also decrease, but the particle TOF of Rou\_str is always higher than that of Wulff\_str. At 700 K, the TOF of Rou\_str is  $5.35 \times 10^6 \text{ s}^{-1} \text{ site}^{-1}$  and that of Wulff\_str is  $8.26 \times 10^5 \text{ s}^{-1} \text{ site}^{-1}$ . At 600 K, the TOF of Rou\_str is  $1.04 \times 10^6 \text{ s}^{-1} \text{ site}^{-1}$ , which is 41.61 times relative to Wulff\_str ( $2.50 \times 10^4 \text{ s}^{-1} \text{ site}^{-1}$ ). This indicates that using the ideal model significantly underestimates the catalytic performance of the catalyst in real reaction environments, especially at low temperatures.

According to 2D activity and the CN maps of NPs (Figure S16), we counted the activity difference on the surface sites with different CNs at 600 K, as shown in Figure 4c. We also plotted the three-dimensional (3D) activity-site maps of Rou\_str and Wulff\_str NPs according to the site TOF per surface site with different CNs (Figure 4d). We observed that the enhanced catalytic activity of Rou\_str is mainly located on the lower CN surface sites, which is consistent with the previous finding that the low-coordinated sites of CO-induced Pt NPs are mainly attributed to the high CO oxidation activity at low temperatures.<sup>51</sup> In particular, small clusters and adatoms show extraordinary activities, and the perimeter sites of the clusters are more active. However, for Wulff\_str, the reaction sites of CN = 8 and 9 show higher activity than Rou\_str, which is due to enough neighborhood coupling sites on the NP surface. The 2D activity–CN maps, activity differences, and 3D activity–site maps of the NPs at 700 and 800 K are shown in Figures S17–S18. The small clusters and adatoms with lower CNs of Rou\_str are still the main activity sources, but these sites do not exist on the surface of Wulff\_str (Figure S19). Therefore, the generation of small clusters and adatoms has a significant impact on catalytic performance, especially at low temperatures, and should be considered as an important factor in the design of low-temperature, high-activity catalysts.

#### 4. CONCLUSIONS

The discovery of self-generated active atomic clusters provides a new understanding of many reaction phenomena. We observed a significant reactivity oscillation for the dynamically reconstructed Pt NPs under a CO pressure of 1000 Pa and an O<sub>2</sub> pressure of 500 Pa at 800 K. The size and location of these clusters and adatoms on the NP surfaces play a crucial role in NP activity changes, where the island clusters are inactive but the peninsula clusters show high activity. Such a reaction oscillation can be referred to as an intrinsic oscillation because it is caused by the spontaneous migration of catalyst surface atoms during the reaction rather than by external environmental changes. Moreover, we found that the small clusters and adatoms formed on the (111) facets turn this inactive surface into an active surface during the reaction. This gives a new perspective to understanding the experimental observations of the enhanced catalytic properties due to the increase in

the number of terrace sites. The number of active low CN sites on the NP surface is normally determined by the corner and edge fractions of the particles. We show that the atomic clusters on the NP facets also contribute active low CN sites to catalytic reactions, which brings new paradigms of catalyst design. Because the reshaping phenomena of metal NPs are common under reaction conditions, the active atomic clusters can be a general factor influencing the catalytic performance of NPs. We may need to re-examine the active sites of NPs because the effect of self-generated clusters has been largely ignored in previous studies. Herein, we point out that tuning reaction environment conditions is a promising strategy for designing highly efficient catalysts with more active sites. In the meantime, when designing the catalyst, we should consider the environmental effects on the catalyst dispersion, accessibility, and stability under different conditions.

Overall, we present an atomic KMC method to simulate nonequilibrium NP transformation on large spatial and temporal scales. Through a kinetic study, we demonstrate that despite the morphology change, the reshaping of metal NP could create atomic clusters on the NP that work as new types of active sites in reactions. These findings provide a new understanding of the nature of active sites on NP surfaces and contribute to the efficient design of catalysts with high catalytic reactivity and durability in the future.

#### ■ ASSOCIATED CONTENT

##### Data Availability Statement

The data that support the plots depicted in the manuscript and other findings of this study are available upon request from the corresponding authors. Demo code can be found on github: [https://github.com/mosp-catalysis/kmc\\_Pt\\_NP\\_CO](https://github.com/mosp-catalysis/kmc_Pt_NP_CO)

##### Supporting Information

The Supporting Information is available free of charge at <https://pubs.acs.org/doi/10.1021/jacsau.4c00088>.

Calculation of rate constants; KMC simulations of surface reconstruction of Pt catalyst and the CO oxidation reaction; adsorption energies of CO and O; reaction energy barrier of CO oxidation; diffusion barriers of CO and O; repulsive interaction of adsorbates; the energy barrier of atomic migration; the metal–metal interaction in a catalyst system; the verification of the formula for the migration barrier of the catalyst surface atom (Table S1); adsorption energies of CO and O, transition state energy of CO oxidation, surface energies and cohesive energy of the catalyst (Figures S1–S2); atomic structures of gas molecule adsorption and lateral interaction adsorbates reaction and diffusion, catalyst atom migration, DFT optimized (Figures S3–S8); related analysis of Pt NP reconstruction in CO environment and in vacuum (Figures S9–S12); maps of adsorption probability, reaction activity, and adsorption coverage, and others in the CO oxidation reaction (Figures S14–S19) (PDF)

#### ■ AUTHOR INFORMATION

##### Corresponding Authors

Beien Zhu – Photon Science Research Center for Carbon Dioxide, Shanghai Advanced Research Institute, Chinese Academy of Sciences, Shanghai 201210, China; [orcid.org/0000-0002-0126-0854](https://orcid.org/0000-0002-0126-0854); Email: [zhube@sari.ac.cn](mailto:zhube@sari.ac.cn)

Yi Gao – Photon Science Research Center for Carbon Dioxide and Key Laboratory of Low-Carbon Conversion Science & Engineering, Shanghai Advanced Research Institute, Chinese Academy of Sciences, Shanghai 201210, China; [orcid.org/0000-0001-6015-5694](https://orcid.org/0000-0001-6015-5694); Email: [gaoyi@sari.ac.cn](mailto:gaoyi@sari.ac.cn)

## Authors

Xiao-Yan Li – Shanghai Institute of Applied Physics, Chinese Academy of Sciences, Shanghai 201800, China; Department of Chemistry, Northwestern University, Evanston, Illinois 60208, United States

Pengfei Ou – Department of Chemistry, Northwestern University, Evanston, Illinois 60208, United States

Xinyi Duan – Shanghai Institute of Applied Physics, Chinese Academy of Sciences, Shanghai 201800, China

Lei Ying – Shanghai Institute of Applied Physics, Chinese Academy of Sciences, Shanghai 201800, China

Jun Meng – Shanghai Institute of Applied Physics, Chinese Academy of Sciences, Shanghai 201800, China; [orcid.org/0000-0002-8976-7464](https://orcid.org/0000-0002-8976-7464)

Complete contact information is available at: <https://pubs.acs.org/10.1021/jacsau.4c00088>

## Author Contributions

B.Z. and Y.G. supervised this project. X.-Y.L. performed all DFT calculations and KMC simulations, wrote KMC program code, and the manuscript. P.O., X.D. and J.M. discussed the results and commented on the manuscript. L.Y. performed the code optimization and demo programming. The manuscript was written through contributions of all authors. All authors have given approval to the final version of the manuscript.

## Funding

This work was supported by the National Key R&D Program of China (2023YFA1506903), National Natural Science Foundation of China (12174408), Natural Science Foundation of Shanghai Municipality (22JC1404200), Shanghai Municipal Science and Technology Major Project, and Foundation of Key Laboratory of Low-Carbon Conversion Science & Engineering, Shanghai Advanced Research Institute, Chinese Academy of Sciences (KLLCCSE-202201Z, SARI, CAS). B.Z. thanks the Key Research Program of Frontier Sciences, CAS, Grant No. ZDBS-LY-7012 for their financial support.

## Notes

The authors declare no competing financial interest.

## ACKNOWLEDGMENTS

The authors are grateful for all funding support. The computational resources utilized in this research were provided by the National Supercomputer Centers in Shanghai and Guangzhou.

## REFERENCES

- (1) Seh, Z. W.; Kibsgaard, J.; Dickens, C. F.; Chorkendorff, I.; Nørskov, J. K.; Jaramillo, T. F. Combining Theory and Experiment in Electrocatalysis: Insights into Materials Design. *Science* **2017**, *355*, No. eaad4998.
- (2) Wu, C.-Y.; Wolf, W. J.; Levartovsky, Y.; Bechtel, H. A.; Martin, M. C.; Toste, F. D.; Gross, E. High-Spatial-Resolution Mapping of Catalytic Reactions on Single Particles. *Nature* **2017**, *541*, 511–515.
- (3) Yuan, W.; Zhu, B.; Li, X.-Y.; Hansen, T. W.; Ou, Y.; Fang, K.; Yang, H.; Zhang, Z.; Wagner, J. B.; Gao, Y.; Wang, Y. Visualizing H<sub>2</sub>O Molecules Reacting at TiO<sub>2</sub> Active Sites with Transmission Electron Microscopy. *Science* **2020**, *367*, 428–430.
- (4) Yuan, W.; Zhu, B.; Fang, K.; Li, X.-Y.; Hansen, T. W.; Ou, Y.; Yang, H.; Wagner, J. B.; Gao, Y.; Wang, Y.; Zhang, Z. In Situ Manipulation of the Active Au-TiO<sub>2</sub> Interface with Atomic Precision during CO Oxidation. *Science* **2021**, *371*, 517–521.
- (5) Jiang, D.; Wan, G.; Stenlid, J. H.; García-Vargas, C. E.; Zhang, J.; Sun, C.; Li, J.; Abild-Pedersen, F.; Tassone, C. J.; Wang, Y. Dynamic and Reversible Transformations of Subnanometre-sized Palladium on Ceria for Efficient Methane Removal. *Nat. Catal.* **2023**, *6*, 618–627.
- (6) Frey, H.; Beck, A.; Huang, X.; van Bokhoven, J. A.; Willinger, M.-G. Dynamic Interplay between Metal Nanoparticles and Oxide Support under Redox Conditions. *Science* **2022**, *376*, 982–987.
- (7) Vendelbo, S. B.; Elkjær, C. F.; Falsig, H.; Puspitasari, I.; Dona, P.; Mele, L.; Morana, B.; Nelissen, B.; Van Rijn, R.; Creemer, J.; et al. Visualization of Oscillatory Behaviour of Pt Nanoparticles Catalysing CO Oxidation. *Nat. Mater.* **2014**, *13*, 884–890.
- (8) Hansen, P. L.; Wagner, J. B.; Helveg, S.; Rostrup-Nielsen, J. R.; Clausen, B. S.; Topsøe, H. Atom-Resolved Imaging of Dynamic Shape Changes in Supported Copper Nanocrystals. *Science* **2002**, *295*, 2053–2055.
- (9) Duan, M.; Yu, J.; Meng, J.; Zhu, B.; Wang, Y.; Gao, Y. Reconstruction of Supported Metal Nanoparticles in Reaction Conditions. *Angew. Chem., Int. Ed.* **2018**, *57*, 6464–6469.
- (10) Zhang, X.; Meng, J.; Zhu, B.; Yu, J.; Zou, S.; Zhang, Z.; Gao, Y.; Wang, Y. In Situ TEM Studies of the Shape Evolution of Pd Nanocrystals under Oxygen and Hydrogen Environments at Atmospheric Pressure. *Chem. Commun.* **2017**, *53*, 13213–13216.
- (11) Zhang, X.; Meng, J.; Zhu, B.; Yuan, W.; Yang, H.; Zhang, Z.; Gao, Y.; Wang, Y. Unexpected Refaceting of Palladium Nanoparticles under Atmospheric N<sub>2</sub> Conditions. *Chem. Commun.* **2018**, *54*, 8587–8590.
- (12) Chee, S. W.; Arce-Ramos, J. M.; Li, W.; Genest, A.; Mirsaidov, U. Structural Changes in Noble Metal Nanoparticles during CO Oxidation and Their Impact on Catalyst Activity. *Nat. Commun.* **2020**, *11*, No. 2133.
- (13) Ghosh, T.; Arce-Ramos, J. M.; Li, W.-Q.; Yan, H.; Chee, S. W.; Genest, A.; Mirsaidov, U. Periodic Structural Changes in Pd Nanoparticles during Oscillatory CO Oxidation Reaction. *Nat. Commun.* **2022**, *13*, No. 6176.
- (14) Jiang, Y.; Li, H.; Wu, Z.; Ye, W.; Zhang, H.; Wang, Y.; Sun, C.; Zhang, Z. In Situ Observation of Hydroge-Induced Surface Faceting for Palladium–Copper Nanocrystals at Atmospheric Pressure. *Angew. Chem., Int. Ed.* **2016**, *55*, 12427–12430.
- (15) Chmielewski, A.; Meng, J.; Zhu, B.; Gao, Y.; Guesmi, H.; Prunier, H.; Alloyeau, D.; Wang, G.; Louis, C.; Delannoy, L.; et al. Reshaping Dynamics of Gold Nanoparticles under H<sub>2</sub> and O<sub>2</sub> at Atmospheric Pressure. *ACS Nano* **2019**, *13*, 2024–2033.
- (16) Chen, B. W. J.; Xu, L.; Mavrikakis, M. Computational Methods in Heterogeneous Catalysis. *Chem. Rev.* **2021**, *121*, 1007–1048.
- (17) Grajciar, L.; Heard, C. J.; Bondarenko, A. A.; Polynski, M. V.; Meeprasert, J.; Pidko, E. A.; Nachtigall, P. Towards Operando Computational Modeling in Heterogeneous Catalysis. *Chem. Soc. Rev.* **2018**, *47*, 8307–8348.
- (18) Yoon, J.; Cao, Z.; Raju, R. K.; Wang, Y.; Burnley, R.; Gellman, A. J.; Farimani, A. B.; Ulissi, Z. W. Deep Reinforcement Learning for Predicting Kinetic Pathways to Surface Reconstruction in a Ternary Alloy. *Mach. Learn.: Sci. Technol.* **2021**, *2*, No. 045018.
- (19) Nørskov, J. K.; Bligaard, T.; Rossmeisl, J.; Christensen, C. H. Towards the Computational Design of Solid Catalysts. *Nat. Chem.* **2009**, *1*, 37–46.
- (20) Martoňák, R.; Laio, A.; Parrinello, M. Predicting Crystal Structures: the Parrinello-Rahman Method Revisited. *Phys. Rev. Lett.* **2003**, *90*, No. 075503.
- (21) Zhu, B.; Xu, Z.; Wang, C.; Gao, Y. Shape Evolution of Metal Nanoparticles in Water Vapor Environment. *Nano Lett.* **2016**, *16*, 2628–2632.

- (22) Zhu, B.; Meng, J.; Yuan, W.; Zhang, X.; Yang, H.; Wang, Y.; Gao, Y. Reshaping of Metal Nanoparticles under Reaction Conditions. *Angew. Chem., Int. Ed.* **2020**, *59*, 2171–2180.
- (23) Kitchin, J. R. Machine Learning in Catalysis. *Nat. Catal.* **2018**, *1*, 230–232.
- (24) Artrith, N.; Kolpak, A. M. Understanding the Composition and Activity of Electrocatalytic Nanoalloys in Aqueous Solvents: a Combination of DFT and Accurate Neural Network Potentials. *Nano Lett.* **2014**, *14*, 2670–2676.
- (25) Liu, M.; Yang, Y.; Kitchin, J. R. Semi-grand Canonical Monte Carlo Simulation of the Acrolein Induced Surface Segregation and Aggregation of AgPd with Machine Learning Surrogate Models. *J. Chem. Phys.* **2021**, *154*, No. 134701, DOI: 10.1063/5.0046440.
- (26) Andersen, M.; Plaisance, C. P.; Reuter, K. Assessment of Mean-Field Microkinetic Models for CO Methanation on Stepped Metal Surfaces Using Accelerated Kinetic Monte Carlo. *J. Chem. Phys.* **2017**, *147*, No. 152705.
- (27) Stamatakis, M.; Vlachos, D. G. Unraveling the Complexity of Catalytic Reactions via Kinetic Monte Carlo Simulation: Current Status and Frontiers. *ACS Catal.* **2012**, *2*, 2648–2663.
- (28) He, X.; Cheng, F.; Chen, Z.-X. The Lattice Kinetic Monte Carlo Simulation of Atomic Diffusion and Structural Transition for Gold. *Sci. Rep.* **2016**, *6*, No. 33128.
- (29) Sumaria, V.; Nguyen, L.; Tao, F. F.; Sautet, P. Atomic-Scale Mmechanism of Platinum Catalyst Restructuring under a Pressure of Reactant gas. *J. Am. Chem. Soc.* **2023**, *145*, 392–401.
- (30) Xu, L.; Papanikolaou, K. G.; Lechner, B. A.; Je, L.; Somorjai, G. A.; Salmeron, M.; Mavrikakis, M. Formation of Active Sites on Transition Metals through Reaction-Driven Migration of Surface Atoms. *Science* **2023**, *380*, 70–76.
- (31) Jørgensen, M.; Grönbeck, H. Scaling Relations and Kinetic Monte Carlo Simulations to Bridge the Materials Gap in Heterogeneous Catalysis. *ACS Catal.* **2017**, *7*, 5054–5061.
- (32) Gillespie, D. T. A General Method for Numerically Simulating the Stochastic Time Evolution of Coupled Chemical Reactions. *J. Comput. Phys.* **1976**, *22*, 403–434.
- (33) Voter, A. F.; Sickafus, K.; Kotomin, E.; Uberuaga, B. In *Radiation Effects in Solids*, NATO Science Series; Springer, Berlin, 2007.
- (34) Reuter, K. First-Principles Kinetic Monte Carlo Simulations for Heterogeneous Catalysis: Concepts, Status, and Frontiers. In *Modeling and Simulation of Heterogeneous Catalytic Reactions: From the Molecular Process to the Technical System*; Deutschmann, O., Ed.; Wiley-VCH, 2012; Chapter 3, pp 71–111.
- (35) Zhu, B.; Qi, R.; Yuan, L.; Gao, Y. Real-Time Atomistic Simulation of the Ostwald Ripening of TiO<sub>2</sub> Supported Au Nanoparticles. *Nanoscale* **2020**, *12*, 19142–19148.
- (36) Han, Y.; Li, X.-Y.; Zhu, B.; Gao, Y. Unveiling the Au Surface Reconstruction in a CO Environment by Surface Dynamics and Ab Initio Thermodynamics. *J. Phys. Chem. A* **2022**, *126*, 6538–6547.
- (37) Li, X. Y.; Zhu, B.; Qi, R.; Gao, Y. Real-Time Simulation of Nonequilibrium Nanocrystal Transformations. *Adv. Theory Simul.* **2019**, *2*, No. 1800127.
- (38) Calle-Vallejo, F.; Martínez, J. I.; García-Lastra, J. M.; Sautet, P.; Loffreda, D. Fast Prediction of Adsorption Properties for Platinum Nanocatalysts with Generalized Coordination Numbers. *Angew. Chem., Int. Ed.* **2014**, *53*, 8316–8319.
- (39) Calle-Vallejo, F.; Loffreda, D.; Koper, M. T.; Sautet, P. Introducing Structural Sensitivity into Adsorption–Energy Scaling Relations by Means of Coordination Numbers. *Nat. Chem.* **2015**, *7*, 403–410.
- (40) Kresse, G.; Hafner, J. Ab Initio Molecular Dynamics for Liquid Metals. *Phys. Rev. B* **1993**, *47*, No. 558.
- (41) Blöchl, P. E.; Först, C. J.; Schimpl, J. Projector Augmented Wave Method: Ab Initio Molecular Dynamics with Full Wave Functions. *Bull. Mater. Sci.* **2003**, *26*, 33–41.
- (42) Perdew, J. P.; Burke, K.; Ernzerhof, M. Generalized Gradient Approximation Made Simple. *Phys. Rev. Lett.* **1996**, *77*, No. 3865.
- (43) Hammer, B.; Hansen, L. B.; Nørskov, J. K. Improved Adsorption Energetics within Density-Functional Theory Using Revised Perdew-Burke-Ernzerhof Functionals. *Phys. Rev. B* **1999**, *59*, No. 7413.
- (44) Gajdoš, M.; Eichler, A.; Hafner, J. CO Adsorption on Close-Packed Transition and Noble Metal Surfaces: Trends from Ab Initio Calculations. *J. Phys.: Condens. Matter* **2004**, *16*, No. 1141.
- (45) Gajdoš, M.; Hafner, J.; Eichler, A. Ab Initio Density-Functional Study of NO on Close-Packed Transition and Noble Metal Surfaces: I. Molecular Adsorption. *J. Phys.: Condens. Matter* **2006**, *18*, No. 13.
- (46) Henkelman, G.; Uberuaga, B. P.; Jónsson, H. A Climbing Image Nudged Elastic Band Method for Finding Saddle Points and Minimum Energy Paths. *J. Chem. Phys.* **2000**, *113*, 9901–9904.
- (47) Monkhorst, H. J.; Pack, J. D. Special Points for Brillouin-Zone Integrations. *Phys. Rev. B* **1976**, *13*, No. 5188.
- (48) Zhu, B.; Meng, J.; Gao, Y. Equilibrium Shape of Metal Nanoparticles under Reactive Gas Conditions. *J. Phys. Chem. C* **2017**, *121*, 5629–5634.
- (49) Avanesian, T.; Dai, S.; Kale, M. J.; Graham, G. W.; Pan, X.; Christopher, P. Quantitative and Atomic-Scale View of CO-Induced Pt Nanoparticle Surface Reconstruction at Saturation Coverage via DFT Calculations Coupled with *In Situ* TEM and IR. *J. Am. Chem. Soc.* **2017**, *139*, 4551–4558.
- (50) Michalka, J. R.; Latham, A. P.; Gezelter, J. D. CO-Induced Restructuring on Stepped Pt Surfaces: A Molecular Dynamics Study. *J. Phys. Chem. C* **2016**, *120*, 18180–18190.
- (51) Neugeboren, J.; Borodin, D.; Hahn, H. W.; Altschäffel, J.; Kandratsenka, A.; Auerbach, D. J.; Campbell, C. T.; Schwarzer, D.; Harding, D. J.; Wodtke, A. M.; Kitsopoulos, T. N. Velocity-Resolved Kinetics of Site-Specific Carbon Monoxide Oxidation on Platinum Surfaces. *Nature* **2018**, *558*, 280–283.